



This discussion paper is/has been under review for the journal Nonlinear Processes in Geophysics (NPG). Please refer to the corresponding final paper in NPG if available.

Isotropy restoration toward high-beta space plasmas

H. Comişel^{1,2}, Y. Narita^{3,4}, and U. Motschmann^{1,5}

¹Institut für Theoretische Physik, Technische Universität Braunschweig, Mendelssohnstr. 3, 38106, Germany

²Institute for Space Sciences, Atomistilor 409, P.O. Box MG-23, Bucharest-Măgurele, 77125, Romania

³Space Research Institute, Austrian Academy of Sciences, Schmiedlstr. 6, 8042 Graz, Austria

⁴Institut für Geophysik und extraterrestrische Physik, Technische Universität Braunschweig, Mendelssohnstr. 3, 38106, Germany

⁵Deutsches Zentrum für Luft- und Raumfahrt, Institut für Planetenforschung, Rutherfordstr. 2, 12489 Berlin, Germany

Received: 10 July 2014 – Accepted: 14 July 2014 – Published: 12 August 2014

Correspondence to: H. Comişel (h.comisel@tu-braunschweig.de)

Published by Copernicus Publications on behalf of the European Geosciences Union & the American Geophysical Union.

[Title Page](#)

[Abstract](#)

[Introduction](#)

[Conclusions](#)

[References](#)

[Tables](#)

[Figures](#)

◀

▶

◀

▶

[Back](#)

[Close](#)

[Full Screen / Esc](#)

[Printer-friendly Version](#)

[Interactive Discussion](#)



Abstract

Wavevector anisotropy of ion-scale plasma turbulence is studied at various values of beta. Two complementary methods are used. One is multi-point measurements of magnetic field in the near-Earth solar wind as provided by the Cluster spacecraft mission, and the other is hybrid numerical simulation of two-dimensional plasma turbulence. The both methods provide evidence of wavevector anisotropy as a function of beta such that isotropy is gradually restored toward higher values of beta. Furthermore, the numerical simulation study demonstrates the existence of scaling law between plasma beta and wavevector anisotropy. This fact can be used to construct a diagnostic tool to determine or to constrain plasma beta using multi-point magnetic field measurements in space.

1 Introduction

Wavevector anisotropy appears in various plasma systems whenever a large-scale magnetic field is imposed. Anisotropy is characterized by extension or elongation of the energy spectrum in the direction parallel or perpendicular to the large-scale field. Examples of wavevector anisotropy can be found in near-Earth solar wind (e.g. Matthaeus et al., 1990; Chen et al., 2012), astrophysical systems such as diffusion of galactic cosmic ray (Bieber et al., 1994, 1996; Ahlers, 2014) and magnetic field decay process in the neutron star crust (Cumming et al., 2004), as well as in laboratory plasmas (Howes et al., 2012; Drake et al., 2013). Development in wavevector anisotropy leads to a structure formation while the plasma evolves into a turbulent state, which is markedly different from fluid turbulence. Evidence of anisotropy in plasma turbulence has also been presented in numerical simulations using different schemes for plasma dynamics such as magnetohydrodynamic (MHD) treatment (Matthaeus et al., 1996; Matthaeus and Gosh, 1999), ion kinetic or hybrid treatment (Comişel et al., 2013; Valentini et al., 2010; Verscharen et al., 2012), gyrokinetic treatment (Howes

NPGD

1, 1313–1330, 2014

Isotropy restoration

H. Comişel et al.

[Title Page](#)

[Abstract](#)

[Introduction](#)

[Conclusions](#)

[References](#)

[Tables](#)

[Figures](#)

◀

▶

◀

▶

[Back](#)

[Close](#)

[Full Screen / Esc](#)

[Printer-friendly Version](#)

[Interactive Discussion](#)



et al., 2011), and full-particle treatment (Chang et al., 2013; Gary et al., 2010; Saito et al., 2010).

Here we propose a scenario that plasma beta is the primary control parameter such that wavevector anisotropy is diminished toward higher values of beta, namely, isotropy restoration. By extending the method and the result obtained in Narita et al. (2014) (hereafter NCM14), we find a transition in the wavevector anisotropy as a function of beta. While the qualitative picture of beta dependence is demonstrated in NCM14, this manuscript presents a more systematic survey of beta dependence both in spacecraft measurements and direct numerical simulations. Our goal is to search for a scaling law of the wavevector anisotropy as a function of beta. Since waves and instabilities in plasmas are known to be dependent on the value of beta, it is natural to assume the existence of mapping or relation between beta and anisotropy. Interestingly, such an idea will lead us to determine or constrain plasma beta using magnetic field measurements only.

The wavevector anisotropy can be quantitatively measured by employing the anisotropy index that compares two covariance quantities, one between the wavevector spectrum and the parallel components of the wavevector and the other between the spectrum and the perpendicular components of the wavevector. The anisotropy index A is defined after Shebalin et al. (1983) as

$$A = \frac{\sum_k k_{\perp}^2 E(k_{\perp}, k_{\parallel})}{\sum_k k_{\parallel}^2 E(k_{\perp}, k_{\parallel})}, \quad (1)$$

where k_{\parallel} and k_{\perp} denote the wavevector components parallel and perpendicular to the large-scale magnetic field, respectively, and $E(k_{\perp}, k_{\parallel})$ the wavevector spectrum. According to this relation, a spectrum is regarded isotropic if the index is unity. Larger values of the index implies that the fluctuation energy is extended to the axis of perpendicular wavevector, while smaller values of the index implies the spectral extension along the axis of parallel wavevector. This index is used as the analysis

Isotropy restoration

H. Comişel et al.

[Title Page](#)[Abstract](#)[Introduction](#)[Conclusions](#)[References](#)[Tables](#)[Figures](#)[◀](#)[▶](#)[◀](#)[▶](#)[Back](#)[Close](#)[Full Screen / Esc](#)[Printer-friendly Version](#)[Interactive Discussion](#)

tool in this work, and we take two independent and complementary approaches to determine the wavevector anisotropy. One is solar wind observations using four-point magnetic field and the other is numerical simulations.

2 Methods

5 2.1 Multi-spacecraft measurements

Four-point magnetic field data sampled by Cluster fluxgate magnetometer in the near-Earth solar wind (Balogh et al., 2001) are used to determine the wavevector spectra. Three time intervals are added to that used in the previous analysis in NCM14: 9 February 2002, 02:10–02:40 UT; 12 February 2002, 14:15–14:45 UT; 18 March 10 2002, 21:30–22:00 UT. The intervals are taken from the solar wind intervals of Cluster measurements under the conditions of nearly regular tetrahedral formation with the minimum inter-spacecraft distance. The magnetic field magnitude, the ion density, the ion bulk speed, and the plasma parameter beta of the three time intervals are listed 15 in Table 1. Ion data are obtained from the ion spectrometry on board Cluster (Rème et al., 2001). With the three added intervals and that used in NCM14, the wavevector spectra are determined at seven different values of beta in the range 0.58–3.66 in the solar wind.

The spectral estimator MSR (Multi-point Signal Resonator) (Narita et al., 2011) is used extensively in the data analysis. The MSR technique is a high-resolution spectral 20 estimator in the wavevector domain using four-point magnetic field data. The method assumes only a set of plane waves, and no additional assumption is needed such as wave modes or Taylor's frozen-in flow hypothesis. Time series of four-point magnetic field data are first transformed into frequencies using the Fast Fourier Transform algorithm. Cross spectral density matrix is then constructed, which is a 12-by-12 25 matrix, consisting of three components of magnetic field and four spatial points, in the frequency domain. This matrix is reduced into a 3-by-3 matrix by projecting onto the

[Title Page](#)[Abstract](#)[Introduction](#)[Conclusions](#)[References](#)[Tables](#)[Figures](#)[◀](#)[▶](#)[◀](#)[▶](#)[Back](#)[Close](#)[Full Screen / Esc](#)[Printer-friendly Version](#)[Interactive Discussion](#)

Isotropy restoration

H. Comişel et al.

Title Page	
Abstract	Introduction
Conclusions	References
Tables	Figures
	
	
Back	Close
Full Screen / Esc	
Printer-friendly Version	
Interactive Discussion	



wavevector domain. The matrix projection is a combination of the minimum variance projection with the MUSIC (Multiple Signal Classification) algorithm (Schmidt, 1986). To complete the projection method, the eigenvalue decomposition of the cross spectral density matrix (Choi et al., 1993) is incorporated.

The wavevector spectra are determined in the following steps. First, the energy spectra for the magnetic field fluctuations are evaluated in the four-dimensional Fourier domain spanned by the frequencies and the wavevectors. Second, the spectra are integrated over the frequencies extended to negative values of frequencies to guarantee the frame-invariance of the wavevector dependence after the frequency integration. Third, the spectra are further reduced into the two-dimensional wavevector domain spanned by the parallel components of wavevector and the perpendicular one by integrating over the directions around the large-scale magnetic field and then summing over the positive and negative components of the parallel wavevector. The two-dimensional wavevector spectra for the three time intervals are displayed in Fig. 1 using the normalization to the proton inertial length by multiplying $\frac{V_A}{\Omega_p}$ (here V_A denotes the Alfvén speed and Ω_p the proton cyclotron frequency). Except for the case at beta 3.66, the measured wavevector spectra are determined at the wavevector components up to $\frac{kV_A}{\Omega_p} = 2.5$. At beta 3.66, the spectrum was determined up to $\frac{kV_A}{\Omega_p} = 1.7$.

The wavevector anisotropy is then evaluated in the reduced spectra using the method of anisotropy index (Eq. 1). The lower limit and the higher limit of the wavenumbers are set to $\frac{kV_A}{\Omega_p} = 0.3$ and $\frac{kV_A}{\Omega_p} = 2.5$, respectively, in the computation of anisotropy index. The lower limit is determined such that the pump waves set in the simulation work (see below) are not counted as anisotropy (the pump waves have the wavenumbers up to $\frac{kV_A}{\Omega_p} = 0.2$). The upper limit is determined such that all intervals (except for beta 3.66) have the same range in the wavenumbers. At beta 3.66, we use the upper limit $\frac{kV_A}{\Omega_p} = 1.7$. For error estimate of the anisotropy index, these wavenumbers are varied by 10 % and this effect is transmitted to computation of the index. The anisotropy profile as a function of beta is displayed in Fig. 3 in the following section.

2.2 Direct numerical simulation

Direct numerical simulation serves as an independent and complementary approach of the anisotropy study. The wavevector anisotropy is studied under six different conditions of beta (0.05, 0.1, 0.2, 0.5, 1.0, and 2.0) covering nearly two orders of magnitude.

- 5 Following the procedure in the observational approach, the wavevector spectra are determined from the numerical simulation of plasma turbulence, and the anisotropy is evaluated using the spectra. However, due to the computational load, we have to limit ourselves to the two-dimensional space spanned by the parallel and the perpendicular directions to the large-scale magnetic field. In this setup, eddies which are intrinsic to
10 fluid-mechanical or gas-dynamic nature of plasmas are suppressed due the lack of the degree of freedom around the large-scale magnetic field. In other words, though the spatial dimensions are two, this numerical setup is advantageous in studying the wave dynamics of plasmas in detail without being influenced by eddies.

Turbulence is produced in the simulation box by solving dynamics of plasma and fields in a step-by-step fashion. We use the hybrid plasma code AIKEF (Adaptive Ion Kinetic Electron Fluid). This code solves a set of Newtonian equation of motion for ions as super-particles under the Coulomb and Lorenz forces together with the Maxwell equations. Electrons are treated as a massless charge-neutralizing fluid (see details on the code in Müller et al. (2011)). In contrast to the analytic approach of solving
15 plasma dynamics, the simulation approach does not require any a-priori knowledge on the statistical property such as a Gaussian distribution of the fluctuating fields nor assumption of the wave modes. The hybrid plasma treatment is suitable particularly for resolving ion kinetic effects as far as electron gyromotion can be neglected, i.e., on the spatial scales between the electron and ion gyroradii (cf. 10–100 km in the solar wind).
20 A disadvantage is that the strong electrostatic effects due to charge localization cannot develop due to the massless electron fluid, as the electrostatic field is immediately canceled out by electrons. However, the charge localization can safely be neglected in our purpose of anisotropy study here.

NPGD

1, 1313–1330, 2014

Isotropy restoration

H. Comişel et al.

[Title Page](#)

[Abstract](#)

[Introduction](#)

[Conclusions](#)

[References](#)

[Tables](#)

[Figures](#)

◀

▶

◀

▶

[Back](#)

[Close](#)

[Full Screen / Esc](#)

[Printer-friendly Version](#)

[Interactive Discussion](#)



Isotropy restoration

H. Comişel et al.

[Title Page](#)[Abstract](#)[Introduction](#)[Conclusions](#)[References](#)[Tables](#)[Figures](#)[◀](#)[▶](#)[◀](#)[▶](#)[Back](#)[Close](#)[Full Screen / Esc](#)[Printer-friendly Version](#)[Interactive Discussion](#)

Implementation of the AIKEF code to our simulation study follows that presented by Verscharen et al. (2012); Comişel et al. (2013) and NCM14. The simulation box has the size 250×250 proton inertial lengths, and is spanned by the parallel to the large-scale magnetic field B_0 (the z direction) and the perpendicular direction (the y direction).

- 5 The large-scale field is constant in space and time. The spatial configuration is two-dimensional, but the vectorial quantities are treated as three-dimensional, e.g., fluctuating magnetic field, electric field, particle velocities. The x direction is pointing out of the simulation plane. Plasma is modeled as the electron-proton plasma.

As the initial condition, a superposition of one-thousand Alfvén waves with random 10 initial phases are set to the system. These pump waves are limited to the wavevectors in the range $\frac{k_{\min} V_A}{\Omega_p} = 0.05$ and $\frac{k_{\max} V_A}{\Omega_p} = 0.2$, in which the fluid picture of plasma is valid. Wavevectors are randomly and isotropically chosen. The amplitude of the pump waves follows Kolmogorov's inertial-range scaling for fluid turbulence, that is, the 15 spectral energy density is set to proportional to $|k|^{-5/3}$. In addition, the total fluctuation amplitude is set to 1 % of the large-scale magnetic field, $\frac{\delta B}{B_0} = 0.01$. To generate the magnetohydrodynamic Alfvén waves, the plasma velocity is set to correlated to the pump wave magnetic field at the initial time. The periodic boundaries are set to the simulation. No fluctuation energy is given externally into the system, neither the fluid-scale range ($\frac{kV_A}{\Omega_p} < 1$) nor the kinetic range ($\frac{kV_A}{\Omega_p} > 1$) during the simulation. Thus, 20 fluctuations (or waves) in the ion-kinetic domain evolve as a consequence of large-scale Alfvén waves.

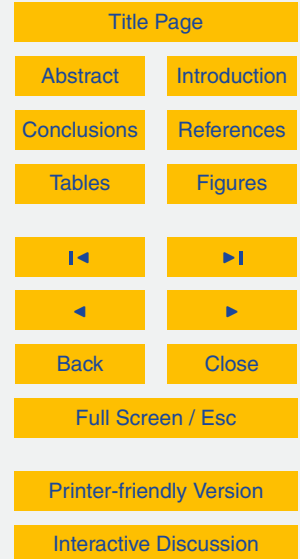
The simulation box is divided into 1024×1024 computational cells. The number of super-particles N per cell are spanning in the range from $N = 400$ to $N = 1600$ per cell while the beta values are in the range between 0.05 and 2.0. We note that the higher 25 value of beta one uses in the simulation, the more particles need to be put into the simulation box. Otherwise many particles may leave the computation cell due to their thermal mobility in the high-beta plasma. This process will eventually lead to a failure in solving the equations of the electromagnetic field when the so-called vacuum cell is

formed in which no ion is stored instantaneously. To carry out a successful run at the value of beta 2.0, a large number of super-particles is set, $N = 1600$, which is a highly-demanding computation.

- The wavevector spectra are determined at 2000 ion gyroperiods ($t\Omega_p = 2000$) by extending the iterations in the simulation run (cf. anisotropy study in NCM14 uses the evolution time at $t\Omega_p = 1000$). This represents the longest possible simulation run for plasma turbulence using the AIKEF code, and the fluctuations reach a quasi-stationary stage at which the fluctuation amplitude, the spectrum, and the anisotropy do not evolve substantially any more. The spectra are obtained by applying the Fast Fourier Transform algorithm to the spatial distribution of magnetic field fluctuations (Fig. 2). Again, the anisotropy index is computed at each value of beta using Eq. (1). The anisotropy-beta relation is displayed in Fig. 3.

3 Results and discussion

- The added solar wind intervals of the Cluster measurements show a diversity (including both similarities and differences) in the contour shapes of the wavevector spectra. First of all, all the three cases exhibit the anisotropy that the spectrum is extended primarily in the direction perpendicular to the large-scale magnetic field. That is, the spectral decay in the wavevector domain is flatter along the perpendicular wavevector axis, while it is steeper along the parallel wavevector axis. Closer look at the spectra yields the following detailed structures. In the case of beta 1.05 (left panel in Fig. 1), the contours of the spectrum are nearly diagonal, connecting a larger value of the parallel component of wavevector to a larger value of the perpendicular one. In the case of beta 1.18, the spectral extension appears not only in the perpendicular direction but also in oblique direction (about 60° from the direction of the large-scale magnetic field). While these two cases show the monotonous spectral decay toward larger values of the wavevector components, the spectrum in the case of beta 3.66 exhibits a formation of the secondary peak along the perpendicular wavevector axis at about $\frac{k_\perp V_A}{\Omega_p} = 0.8$.



Isotropy restoration

H. Comişel et al.

[Title Page](#)[Abstract](#)[Introduction](#)[Conclusions](#)[References](#)[Tables](#)[Figures](#)[Back](#)[Close](#)[Full Screen / Esc](#)[Printer-friendly Version](#)[Interactive Discussion](#)

and the third peak in the oblique direction at about $(\frac{k_{\perp}V_A}{\Omega_p}, \frac{k_{\parallel}V_A}{\Omega_p}) = (1.6, 1.2)$. The spectral decay in the wavevector domain is rather flat in the third case. The evaluated anisotropy index is about 1.8 (at beta 1.05), 2.3 (at beta 1.18), and 2.1 (at beta 3.66). These values are plotted in Fig. 3 together with that already obtained in NCM14 (5.7 at beta 0.58, 3.3 at beta 0.76, 2.3 at beta 1.66, and 2.3 at beta 2.53).

The wavevector spectra obtained from the numerical simulations provide another kind of diversity in the contour shapes. Again, the primary extension of the spectrum appears along the perpendicular wavevector direction (the spectral decay is flatter in the perpendicular direction, and steeper in the parallel direction). Still, the secondary peak is formed along the parallel wavevector axis (e.g., $1 < \frac{k_{\parallel}V_A}{\Omega_p} < 2$ at beta 0.2, $2 < \frac{k_{\parallel}V_A}{\Omega_p} < 3.5$ at beta 1.0). It is also interesting to note that the contour shape at smaller values of the perpendicular wavevector component exhibits a similarity in that there is a hump or a spectral extension, e.g., the transitions from $(\frac{k_{\perp}V_A}{\Omega_p}, \frac{k_{\parallel}V_A}{\Omega_p}) = (0.5, 2.8)$ at beta 0.05 to $(\frac{k_{\perp}V_A}{\Omega_p}, \frac{k_{\parallel}V_A}{\Omega_p}) = (0.5, 4.0)$ at beta 0.2, and further to $(\frac{k_{\perp}V_A}{\Omega_p}, \frac{k_{\parallel}V_A}{\Omega_p}) = (0.5, 5.0)$ at beta 0.5. In contrast, at larger values of the perpendicular wavevector component, the spectral contours do not vary across the parallel wavevector component. The anisotropy index is obtained for the wavevector spectra from the numerical simulations as 4.3 (at beta 0.05), 4.0 (at beta 0.1), 3.4 (at beta 0.2), 2.5 (at beta 0.5), 2.1 (at beta 1.0), and 1.7 (at beta 2.0) (also displayed in Fig. 3).

The anisotropy index plotted as a function of beta on the logarithmic scale (Fig. 3) is suggestive of isotropy restoration at higher values of beta. Both the spacecraft measurements and the numerical simulations show that the anisotropy is stronger (i.e., the spectral decay is steeper along the parallel wavevector axis) when beta is below unity, and is moderate and asymptotes slowly to isotropy ($A \rightarrow 1$) when beta is above unity. However, the quantitative picture of the beta-dependence is different between the observations and the simulations. In the spacecraft measurements in the solar wind, the anisotropy index falls down rather abruptly in the range of beta from 0.5

Isotropy restoration

H. Comişel et al.

Title Page	
Abstract	Introduction
Conclusions	References
Tables	Figures
	
	
Back	Close
Full Screen / Esc	
Printer-friendly Version	
Interactive Discussion	



to 1, and then forms a plateau with only moderate decrease in the anisotropy index. Furthermore, the anisotropy index measured in the solar wind tends to higher than that from the simulations. The wavevector anisotropy from the simulations shows a smooth transition from the low-beta to the high-beta regime. The anisotropy index from the simulations exhibits a nearly power-law scaling in the form $A \propto \beta^{-\alpha}$. The slope in the scaling can be determined by the fitting procedure, and we obtain the empirical scaling law of anisotropy as

$$A = 2.035 \times \beta^{-0.295} \quad (2)$$

Namely, the slope value is close to -0.3 . The scaling law $\beta^{-0.3}$ is superposed to the anisotropy index from the simulations in Fig. 3 for comparison. Except for the smallest value of beta (0.05), the scaling law explains the simulation results with only small deviation.

What is the reason of the difference in the anisotropy index profile (or slope) between the observations and the simulations? We interpret that this difference comes from the spatial dimensions in plasma dynamics. The simulations are limited to two-dimensional spatial setup, and the motion around the large-scale magnetic field is forbidden. Eddies are suppressed in the simulation in the both two planes, the plane perpendicular to the large-scale field (or the plane spanned by the x and y directions) and that spanned by the parallel and perpendicular directions (the y and z directions). Therefore, fluctuations in the simulations represent either electromagnetic waves that propagate or non-eddy spatial structures that do not propagate. In such an ideal setup, two-dimensional plasma exhibits a self-organization or systematic transition of the wavevector anisotropy into isotropy toward higher values of beta.

4 Conclusions

Our work provides evidence that the wavevector anisotropy is stronger in low-beta plasmas, and weaker in high-beta plasmas, which justifies the earlier study in NCM14. Furthermore, in the case of two-dimensional plasmas, there exists a scaling law between the anisotropy index and the plasma parameter beta. Magnetized plasma exhibits a tendency to restore isotropy in the wavevector domain gradually toward higher values of beta. This fact, however, should not be taken as surprising when considering that the role of magnetic field is weaker in high-beta plasmas. We observe the primary extension of the wavevector spectrum in the perpendicular direction to the large-scale magnetic field, which supports the notion of filamentation process in structure formation.

What determines the scaling slope $\alpha \simeq 0.3$ will be a subject of theoretical studies. It may be worth while to compare with the other observational fact that the variance anisotropy (which is a measure of compressibility in magnetic field fluctuations) also exhibits a power-law scaling to beta with the slope -0.56 (Smith et al., 2006).

We point out that the logics in our work can be reversed, that is, the scaling law can be applied to measurements of magnetic field as a diagnostic tool of beta. At the current stage, such a method is applicable in two-dimensional plasmas. Still, the method can be used to constrain the value of beta in three-dimensional plasmas as well. An interesting extension would be an application to astrophysical systems. If such a scaling exists in the magnetohydrodynamic picture of plasmas, one may obtain or constrain the value of beta by analyzing photometry data of filament structures in interstellar media or astrophysical jets.

Author contribution

H. Comişel: simulation, analysis, writing. Y. Narita: observation, analysis, writing. U. Motschmann: coordination, interpretation.

NPGD

1, 1313–1330, 2014

Isotropy restoration

H. Comişel et al.

[Title Page](#)

[Abstract](#)

[Introduction](#)

[Conclusions](#)

[References](#)

[Tables](#)

[Figures](#)

◀

▶

◀

▶

[Back](#)

[Close](#)

[Full Screen / Esc](#)

[Printer-friendly Version](#)

[Interactive Discussion](#)



Acknowledgements. H. Comișel acknowledges Daniel Verscharen for comments and suggestions. This is financially supported by Collaborative Research Center 963, *Astrophysical Flow, Instabilities, and Turbulence* of the German Science Foundation and FP7 313038 STORM of European Commission. We also acknowledge North-German Supercomputing Alliance (Norddeutscher Verbund zur Förderung des Hoch- und Höchstleistungsrechnens – HLRN) for supporting direct numerical simulations.

References

- Ahlers, M.: Anomalous anisotropies of cosmic rays from turbulent magnetic fields, *Phys. Rev. Lett.*, 112, 021101, doi:10.1103/PhysRevLett.112.021101, 2014. 1314
- Balogh, A., Carr, C. M., Acuña, M. H., Dunlop, M. W., Beek, T. J., Brown, P., Fornaçon, K.-H., Georgescu, E., Glassmeier, K.-H., Harris, J., Musmann, G., Oddy, T., and Schwingenschuh, K.: The Cluster Magnetic Field Investigation: overview of in-flight performance and initial results, *Ann. Geophys.*, 19, 1207–1217, doi:10.5194/angeo-19-1207-2001, 2001. 1316
- Bieber, J. W., Matthaeus, W. H., Smith, C. W., Wanner, W., Kallenrode, M.-B., and Wibberenz, G.: Proton and electron mean free paths: the Palmer consensus revisited, *Astrophys. J.*, 420, 294–306, doi:10.1086/173559, 1994. 1314
- Bieber, J. W., Wanner, W., and Matthaeus, W. H.: Dominant two-dimensional solar wind turbulence with implications for cosmic ray transport, *J. Geophys. Res.*, 101, 2511–2522, doi:10.1029/95JA02588, 1996. 1314
- Chang, O., Gary, S. P., and Wang, J.: Whistler turbulence at variable electron beta: three-dimensional particle-in-cell simulations, *J. Geophys. Res.-Space*, 118, 2824–2833, doi:10.1002/jgra.50365, 2013. 1315
- Chen, C. H. K., Mallet, A., Schekochihin, A. A., Horbury, T. S., Wicks, R. T., and Bale S. D.: Three-dimensional structure of solar wind turbulence, *Astrophys. J.*, 758, 120, doi:10.1088/0004-637X/758/2/120, 2012. 1314
- Choi, J., Song, I., and Kim, H. M.: On estimating the direction of arrival when the number of signal sources is unknown, *Signal Process.*, 34, 193–205, 1993. 1317

Isotropy restoration

H. Comișel et al.

[Title Page](#)

[Abstract](#)

[Introduction](#)

[Conclusions](#)

[References](#)

[Tables](#)

[Figures](#)

◀

▶

◀

▶

[Back](#)

[Close](#)

[Full Screen / Esc](#)

[Printer-friendly Version](#)

[Interactive Discussion](#)



Isotropy restoration

H. Comişel et al.

[Title Page](#)[Abstract](#)[Introduction](#)[Conclusions](#)[References](#)[Tables](#)[Figures](#)[◀](#)[▶](#)[◀](#)[▶](#)[Back](#)[Close](#)[Full Screen / Esc](#)[Printer-friendly Version](#)[Interactive Discussion](#)

- Comişel, H., Verscharen, D., Narita, Y., and Motschmann, U.: Spectral evolution of two-dimensional kinetic plasma turbulence in the wavenumber-frequency domain, *Phys. Plasmas*, 20, 090701, doi:10.1063/1.4820936, 2013. 1314, 1319
- Cumming, A., Arras, P., and Zweibel, E.: Magnetic field evolution in neutron star crusts due to the Hall effect and Ohmic decay, *Astrophys. J.*, 609, 999–1017, doi:10.1086/421324, 2004. 1314
- Drake, D. J., Schroeder, J. W. R., Howes, G. G., Kletzing, C. A., Skiff, F., Carter, T. A., and Auerbach, D. W.: Alfvén wave collisions, the fundamental building block of plasma turbulence. I V. Laboratory experiment, *Phys. Plasmas*, 20, 072901, doi:10.1063/1.4813242, 2013. 1314
- Gary, S. P., Saito, S., and Narita, Y.: Whistler turbulence wavevector anisotropies: particle-in-cell simulations, *Astrophys. J.*, 716, 1332, doi:10.1088/0004-637X/716/2/1332, 2010. 1315
- Howes, G. G., Tenbarge, J. M., Dorland, W., Quataert, E., Schekochihin, A. A., Numata, R., and Tatsuno T.: Gyrokinetic simulations of solar wind turbulence from ion to electron scales, *Phys. Rev. Lett.*, 107, 035004, doi:10.1103/PhysRevLett.107.035004, 2011. 1314
- Howes, G. G., Drake, D. J., Nielson, K. D., Carter, T. A., Kletzing, C. A., and Skiff, F.: Toward astrophysical turbulence in the laboratory, *Phys. Rev. Lett.*, 109, 255001, doi:10.1103/PhysRevLett.109.255001, 2012. 1314
- Matthaeus, W. H., Goldstein, M. L., and Roberts, D. A.: Evidence for the presence of quasi-two-dimensional nearly incompressible fluctuations in the solar wind, *J. Geophys. Res.*, 95, 20673–20683, doi:10.1029/JA095iA12p20673, 1990. 1314
- Matthaeus, W. H., Gosh, S., Oughton, S., and Roberts, D. A.: Anisotropic three-dimensional MHD turbulence, *J. Geophys. Res.*, 101, 7619–7629, doi:10.1029/95ja03830, 1996. 1314
- Matthaeus, W. H. and Gosh, S.: Spectral decomposition of solar wind turbulence: three-component model, *AIP Conf. Proc.*, The solar wind nine conference, 5–9 October 1998, Nantucket, Massachusetts, 471, 519, doi:10.1063/1.58688, 1999. 1314
- Müller, J., Simon, S., Motschmann, U., Schüle, J., Glassmeier, K.-H., and Pringle, G. J.: Adaptive hybrid model for space plasma simulations, *Comp. Phys. Comm.*, 182, 946, doi:10.1016/j.cpc.2010.12.033, 2011. 1318
- Narita, Y., Glassmeier, K.-H., and Motschmann, U.: High-resolution wave number spectrum using multi-point measurements in space – the Multi-point Signal Resonator (MSR) technique, *Ann. Geophys.*, 29, 351–360, doi:10.5194/angeo-29-351-2011, 2011. 1316
- Narita, Y., Comişel, H., and Motschmann, U.: Spatial structure of ion-scale plasma turbulence, *Front. Physics*, 2, 13, doi:10.3389/fphy.2014.00013, 2014. 1315, 1327

- Rème, H., Aoustin, C., Bosqued, J. M., Dandouras, I., Lavraud, B., Sauvaud, J. A., Barthe, A., Bouyssou, J., Camus, Th., Coeur-Joly, O., Cros, A., Cuvilo, J., Ducay, F., Garbarowitz, Y., Medale, J. L., Penou, E., Perrier, H., Romefort, D., Rouzaud, J., Vallat, C., Alcaydé, D., Jacquey, C., Mazelle, C., d'Uston, C., Möbius, E., Kistler, L. M., Crocker, K., Granoff, M., Mouikis, C., Popecki, M., Vosbury, M., Klecker, B., Hovestadt, D., Kucharek, H., Kuenneth, E., Paschmann, G., Scholer, M., Sckopke, N., Seidenschwang, E., Carlson, C. W., Curtis, D. W., Ingraham, C., Lin, R. P., McFadden, J. P., Parks, G. K., Phan, T., Formisano, V., Amata, E., Bavassano-Cattaneo, M. B., Baldetti, P., Bruno, R., Chionchio, G., Di Lellis, A., Marcucci, M. F., Pallocchia, G., Korth, A., Daly, P. W., Graeve, B., Rosenbauer, H., Vasyliunas, V., McCarthy, M., Wilber, M., Eliasson, L., Lundin, R., Olsen, S., Shelley, E. G., Fuselier, S., Ghielmetti, A. G., Lennartsson, W., Escoubet, C. P., Balsiger, H., Friedel, R., Cao, J.-B., Kovrashkin, R. A., Papamastorakis, I., Pellat, R., Scudder, J., and Sonnerup, B.: First multispacecraft ion measurements in and near the Earth's magnetosphere with the identical Cluster ion spectrometry (CIS) experiment, *Ann. Geophys.*, 19, 1303–1354, doi:10.5194/angeo-19-1303-2001, 2001. 1316
- Saito, S., Gary, S. P., and Narita, Y.: Wavenumber spectrum of whistler turbulence: particle-in-cell simulation, *Phys. Plasmas*, 17, 122316, doi:10.1063/1.3526602, 2010. 1315
- Schmidt, R. O.: Multiple emitter location and signal parameter estimation, *IEEE T. Antenn. Propag.*, AP-34, 276–280, 1986. 1317
- Shebalin, J. V., Matthaeus, W. H., and Montgomery, D.: Anisotropy in MHD turbulence due to a mean magnetic field, *J. Plasma Phys.*, 29, 525, doi:10.1017/S0022377800000933, 1983. 1315
- Smith, C. W., Vasquez, B. J., and Hamilton, K.: Interplanetary magnetic fluctuation anisotropy in the inertial range, *J. Geophys. Res.*, 111, A09111, doi:10.1029/2006JA011651, 2006. 1323
- Valentini, F., Califano, F., and Veltri, P.: Two-dimensional kinetic turbulence in the solar wind, *Phys. Rev. Lett.*, 104, 205002, doi:10.1103/PhysRevLett.104.205002, 2010. 1314
- Verscharen, D., Marsch, E., Motschmann, U., and Müller, J.: Kinetic cascade beyond magnetohydrodynamics of solar wind turbulence in two-dimensional hybrid simulations, *Phys. Plasmas*, 19, 022305, doi:10.1063/1.3682960, 2012. 1314, 1319

Isotropy restoration

H. Comişel et al.

[Title Page](#)[Abstract](#)[Introduction](#)[Conclusions](#)[References](#)[Tables](#)[Figures](#)[Back](#)[Close](#)[Full Screen / Esc](#)[Printer-friendly Version](#)[Interactive Discussion](#)

Isotropy restoration

H. Comişel et al.

[Title Page](#)[Abstract](#)[Introduction](#)[Conclusions](#)[References](#)[Tables](#)[Figures](#)[◀](#)[▶](#)[◀](#)[▶](#)[Back](#)[Close](#)[Full Screen / Esc](#)[Printer-friendly Version](#)[Interactive Discussion](#)

Table 1. Magnetic field magnitude B_0 , ion number density n_i , flow speed V , and plasma beta for ions of the solar wind data added to that in Narita et al. (2014). Items are sorted in ascending order of beta.

Date	Interval	B_0 nT	n_i cm^{-3}	V km s^{-1}	beta
9 Feb 2002	02:10–02:40 UT	4.7	3.7	493.1	1.05
12 Feb 2002	14:15–14:45 UT	6.4	3.3	512.8	1.18
18 Mar 2002	21:30–22:00 UT	10.9	15.5	446.3	3.66

Isotropy restoration

H. Comişel et al.

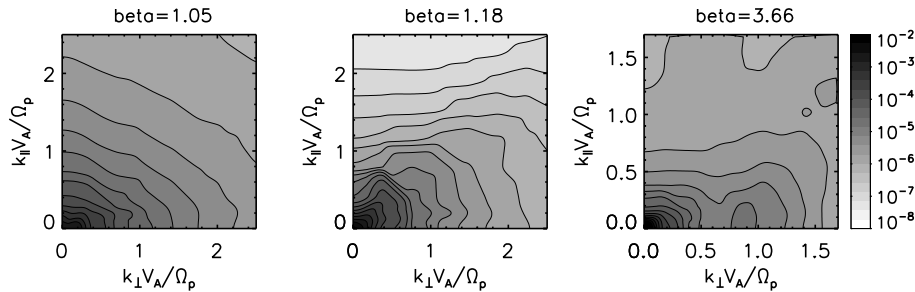


Figure 1. Magnetic energy spectra in the plane spanned by the perpendicular and parallel components of the wavevectors with respect to the large-scale magnetic field measured by Cluster spacecraft in the solar wind.

- [Title Page](#)
- [Abstract](#) [Introduction](#)
- [Conclusions](#) [References](#)
- [Tables](#) [Figures](#)
-
-
- [Full Screen / Esc](#)
- [Printer-friendly Version](#)
- [Interactive Discussion](#)



Isotropy restoration

H. Comişel et al.

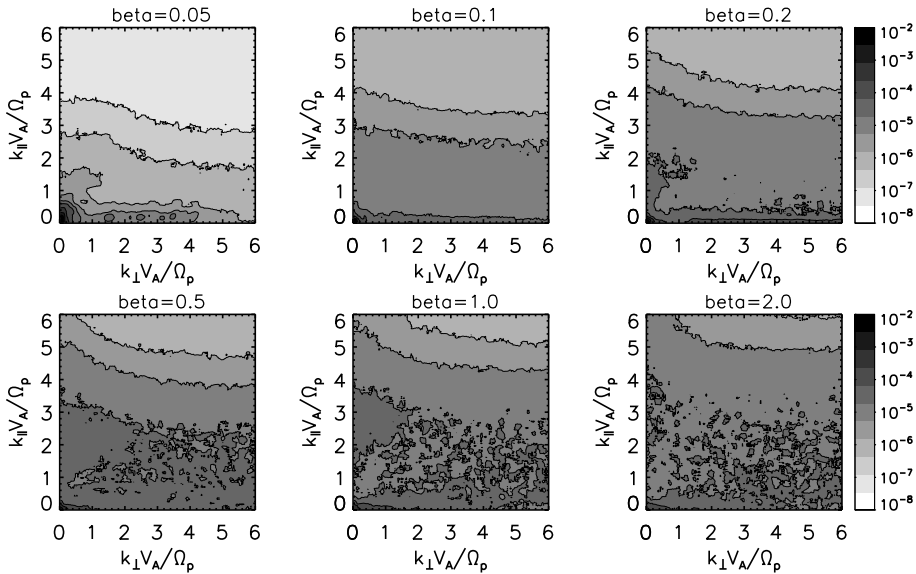


Figure 2. Magnetic energy spectra obtained by numerical simulation of two-dimensional ion-scale plasma turbulence at a late-stage time evolution (2000 ion gyroperiods). The panel styles are the same as that in Fig. 1.

- [Title Page](#)
- [Abstract](#) [Introduction](#)
- [Conclusions](#) [References](#)
- [Tables](#) [Figures](#)
- [◀](#) [▶](#)
- [◀](#) [▶](#)
- [Back](#) [Close](#)
- [Full Screen / Esc](#)
- [Printer-friendly Version](#)
- [Interactive Discussion](#)



Isotropy restoration

H. Comişel et al.

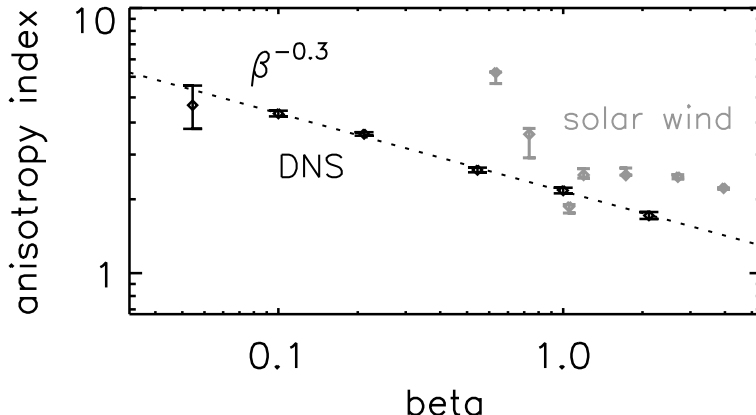


Figure 3. Beta dependence of anisotropy index obtained by the Cluster spacecraft measurements in the solar wind (in gray) and that by direct numerical simulation (DNS, in black) with the power-law fitting.

- [Title Page](#)
- [Abstract](#) [Introduction](#)
- [Conclusions](#) [References](#)
- [Tables](#) [Figures](#)
- [◀](#) [▶](#)
- [◀](#) [▶](#)
- [Back](#) [Close](#)
- [Full Screen / Esc](#)
- [Printer-friendly Version](#)
- [Interactive Discussion](#)

